PALEOCEANOGRAPHY, VOL. 13, NO. 4, PAGES 340-351, AUGUST 1998

Simulations of two last glacial maximum ocean states

Grant R. Bigg and Martin R. Wadley

School of Environmental Sciences, University of East Anglia, Norwich, England, United Kingdom

David P. Stevens and John A. Johnson

School of Mathematics, University of East Anglia, Norwich, England, United Kingdom

Abstract. Two stable thermohaline circulation states were produced in simulations of the last glacial maximum (LGM) ocean, both forced by the same prescribed atmosphere. Direct application of this atmosphere led to an equilibrium state with strong North Atlantic Deep Water formation (northern sinking state (NSS)). Upon applying a weak freshwater flux anomaly to the North Atlantic for a short time a state was entered with little North Atlantic, but significant Southern Ocean, Deep Water formation (southern sinking state (SSS)). A fully dynamic and thermodynamic iceberg trajectory model was developed, and icebergs were seeded into both states. Distinctly different pathways were found, particularly in the eastern Atlantic where the SSS icebergs tend to move south along the European coast while they move north in the NSS. While neither ocean state is claimed to be a definitive model for the LGM ocean, paleoclimate data are more consistent with the characteristics of the NSS.

1. Introduction

The thermohaline circulation of the global ocean is responsible for a significant amount of the poleward heat transport required to maintain the equitable climate of the planet. Variation in the strength and structure of this circulation influences regional or even global climate. Current uncertainty over the state of the thermohaline circulation at the last glacial maximum (LGM) is therefore of fundamental importance in understanding glacial climate. *Boyle* [1995] and *Yu et al.* [1996] have summarized the three conceptual models which presently have claims within the literature, both, nevertheless, opting for a scenario where the production of Glacial North Atlantic Deep and Intermediate Water (GNAIW) was of similar magnitude to today, albeit with more flux at shallower depths. Here it is worth summarizing the arguments for each model to set the scene for the numerical experiments described in this paper.

The first interpretation has all the LGM global ocean's deep water formed in the Southern Ocean (Circumpolar Deep Water (CPDW)). From there it spread out into the Atlantic, Indian, and Pacific Oceans to form the basis for all deep and intermediate water masses. Some convection occurred in both the North Atlantic and North Pacific, but water masses formed in both of these areas remained at relatively shallow depths. This construction has arisen from nutrient-related interpretations of benthic $\delta^{13}C$. Higher concentrations of nutrients in Indo-Pacific Deep Water (IPDW) than in CPDW were taken to imply the absence of the present-day conveyor belt and the presence of some Pacific convection [*Lynch-Stieglitz and Fairbanks*, 1994]. Shallow convection in the Atlantic was also implied by nutrient-depleted waters entering the Caribbean at intermediate depths [*Boyle and Keigwin*, 1987].

Paper number 98PA00402.
0883-8305/98/98PA-00402$12.00

The second construction is an alternative interpretation of this data, presented by *Imbrie et al.* [1992], whereby intermediate water was only formed in the North Atlantic but spread, at these levels, into all the other oceans, except the Southern Ocean. Deep, nutrient-enriched water formed in the latter but remained isolated or spread out only into the deepest parts of the other basins. This would allow the gradient of nutrient enrichment observed between the Atlantic and Pacific [*Zahn et al.*, 1987] and would be compatible with the $\delta^{13}C$ distributions mentioned above.

These interpretations of $\delta^{13}C$ distributions, however, do not rest easily with the radiocarbon ages of LGM deep Atlantic and Pacific waters, which suggest that the ventilation of these oceans occurred at similar rates to today [*Shackleton et al.*, 1988; *Broecker et al.*, 1990]. They are also contrary to Cd/Ca distributions, another nutrient tracer, and radiochemical data. Both the former and the latter suggest that nutrient values of CPDW remained intermediate between Atlantic and Pacific Deep Waters and that GNAIW combined with CPDW in the deep waters exported to the Indian and Pacific Oceans as today [*Boyle*, 1992; *Yu et al.*, 1996]. The numerical model of *Seidov et al.* [1996] also suggests that there was significant deep water production in the North Atlantic at the LGM, but the restriction of this model to the northern Atlantic and the surface relaxation conditions limit the capacity of this model to show a state with deep water formation outside of its domain. In this paper we present two global numerical ocean model simulations, obtained using the same basic atmospheric forcing but with radically different thermohaline circulations, that give guides to specific key geographic areas that can be used to differentiate between the states.

2. Model Details

2.1. Ocean Model

The ocean model configuration has been described by M.R.Wadley et al. (Multiple states in present day and last glacial maximum global simulations forced by a prescribed atmosphere,

hereinafter referred to as Wadley et al., unpublished manuscript, 1997) in terms of a more general study of multiple ocean equilibria in both present-day and LGM conditions. Wadley et al. (unpublished manuscript, 1997) showed that the basic model, relaxed to present-day temperature and salinity, gave a realistic flow field if a somewhat weak thermohaline circulation. However, various other present-day states with deep water formation of varying strength in the North Atlantic and/or Southern Ocean were also obtainable. In this paper we consider the LGM states in much greater depth and explore their implications for resolution of the debate outlined in the Introduction. Wadley et al.'s (unpublished manuscript, 1997) present-day state with vigorous deep water formation in the Greenland Sea (present-day Greenland (PDG)) is used as a modern day analog when appropriate. A short description of the model follows.

The basic ocean model was the Modular Ocean Model (MOM), a primitive equation ocean model [*Pacanowski et al.*, 1991], with a global horizontal resolution of 4° longitude by 3° latitude and 19 levels in the vertical, increasing in thickness with depth. A fine-scale topographic data set [*U.S. Naval Oceanographic Office*, 1983] was used to determine the depth at each horizontal grid point but with the depth set to that locally observed over sills between basins. In addition, the *Peltier* [1994] ice sheet topography was used to determine the coastline at the LGM, with ocean depths shallower by 120 m than today, as is consistent with the reconstructed LGM sea level of *Fairbanks* [1989]. A one grid box island was placed at the North Pole to eliminate the polar singularity associated with standard latitude-longitude coordinates, and Fourier filtering over latitudes poleward of 75° removed the numerical instability caused by converging meridians. Horizontal mixing coefficients for momentum and tracers (temperature and salinity) were 1×10^5 m^2 s^{-1} and 2×10^3 m^2 s^{-1} respectively, while vertical mixing for the tracers increased linearly with depth from 1×10^{-5} m^2 s^{-1} at the surface to 1.5×10^{-4} m^2 s^{-1} at 5000 m [*Krauss*, 1990]. The vertical mixing coefficient for momentum was 1×10^{-5} m^2 s^{-1} for all depths. The accelerated time stepping method of *Bryan* [1984] is used, allowing the time step for the tracers to increase with depth from 2 days at the surface to 16 days below 4100 m. This allows millenial-scale runs to be made at the expense of a restriction to annual mean forcing. A simple thermodynamic sea ice model [*Semtner*, 1976] predicts ice and snow thickness and the surface temperature of the sea ice. The model was initialized with the modern day annual mean temperature [*Levitus et al.*, 1994] and salinity [*Levitus and Boyer*, 1994] with an upward adjustment of the latter of 1 practical salinity unit (psu) to reflect the lower sea level.

The annual mean atmosphere from the LGM paleoclimate simulation of *Hall et al.* [1996] was used to provide the forcing wind stress and the prescribed state from which the surface longwave sensible and latent heat fluxes were calculated from bulk aerodynamic formulae, as detailed in *Bigg* [1994]. This allows the fluxes to adjust to changes in ocean temperature but with an effective thermal coupling sensitivity (20 W m^{-2} K^{-1}) which is greater than that at basin scale (3 W m^{-2} K^{-1} [*Rahmstorf and Willebrand*, 1995]. The consequences of this are limited in the subtropics but accentuate model inaccuracies in regions of deep water formation where fluxes are large. The solar flux is prescribed from the annual mean atmospheric state. Evaporation is given by the mass flux associated with the latent heat term; the divergence associated with this freshwater flux is represented by a potential function [*Huang*, 1993] which has been shown to be important in modeling realistic modern day circulations in regions of surface water imbalance [*Wadley et al.*, 1996]. Of the other elements in the surface water balance, precipitation is imposed by the prescribed atmosphere, and runoff is calculated by letting the net precipitation over land (precipitation less evaporation) flow instantaneously down the steepest local gradient.

The ocean model was run for 2000 years until a quasi-steady state was reached in which vigorous deep water formation occurred in the North Atlantic. This will be known as the northern sinking state (NSS). A LGM state with no North Atlantic Deep Water formation was obtained by perturbing the NSS through an increase of 1 mm/d in the freshwater flux over the North Atlantic north of 42°N and a globally balancing decrease elsewhere for 500 years. The anomaly was then removed, and the model was run on for a further 2000 years. The Atlantic overturning rapidly collapsed after the perturbation was imposed, to be replaced by a state with deep water formation occurring only in the Southern Ocean. This was maintained after the removal of the perturbation: the resulting equilibrium state will be known as the southern sinking state (SSS). To examine the circulations in greater detail, and particularly to provide input to the iceberg model, these equilibrium states were used as the relaxation constraints in 1 year simulations of a robust mode [*Sarmiento and Bryan*, 1982] finer-resolution (1°x1°) model with the same number of vertical levels. Note that both the LGM NSS and SSS are compatible with essentially the same prescribed atmosphere for millenia. This possibility of ocean models supporting multiple states has been shown previously in other situations [e.g., *Bryan*, 1986; *Power and Kleeman*, 1993].

2.2. Iceberg Model

As a means of differentiating between the two model states in a paleoceanographically useful manner, icebergs were seeded into the fine-resolution ocean circulation of both states. The iceberg trajectory model contains full dynamical and thermodynamical evolution of a suite of berg sizes from a given set of release points. The model has been fully described and tested for the present-day North Atlantic and Arctic Oceans by *Bigg et al.* [1997] and is successful in reproducing the present iceberg limits in these oceans [*Bigg et al.*, 1996]. The dynamics in the model derive from *Smith* [1993], who took an iceberg to be affected by the pressure gradient force, the Coriolis force, water drag, air drag and wave drag, with the addition of sea ice drag, a stability criterion permitting the iceberg to roll onto its side [*Weeks and Mellor*, 1978], and a revised expression for the pressure gradient force. A major difference between this model and that used by earlier workers, such as *Matsumoto* [1996, 1997], is the inclusion of a nonlinear term in this pressure gradient force. *Bigg et al.* [1996] showed that this term is crucial for the reproduction of modern iceberg limits because it allows present-day icebergs to be advected sufficiently far in strong but narrow boundary currents such as the Labrador and East Greenland Currents. A range of processes are involved in the melting of icebergs, and each of these has been separately parameterized in the trajectory model [*Bigg et al.*, 1997]. The processes included are turbulent heat transfer, buoyant convection, wave erosion, solar and sensible heating, and sublimation. Icebergs are also allowed to grow through the accumulation of snow from precipitation when the air

temperature is below 0°C. The dominant melting term is that due to wave erosion [*Bigg et al.*, 1997]. The predicted lifetime distribution of the model matches that observed today, confirming the success of the thermodynamic scheme.

Each iceberg is moved according to an integration of its momentum equation over time steps of 135 s, with melting over the time step accruing at its end to give new berg dimensions for the beginning of the next step. The forcing fields are taken from the prescribed atmosphere and the oceanic fields for each of the two states' fine-resolution simulations. If a berg grounds, it is allowed to melt in situ until its draught reduces sufficiently for it to float and move away. If a berg collides with a coastline, it is assumed to be permanently stranded.

To initialize the trajectory model, we needed to determine the location and size distribution of iceberg releases at the LGM. The iceberg flux issuing from all points of the northern hemisphere ice sheets was calculated by taking a modern statistical relationship between glacier calving and net precipitation over Greenland and applying this to the net precipitation [*Hall et al.*, 1996] over the drainage basins of the 21 ka ice sheet reconstruction [*Peltier*, 1994]. A subset of the resulting regional fluxes which was likely to affect the North Atlantic was used to initialize the iceberg flux into the two LGM ocean states; this is shown in Figure 1. The total flux from the eastern coast of North America is only about half that estimated by *Dowdeswell et al.* [1995] or *Matsumoto* [1997], with significantly less from the Hudson Bay area. This is mostly due to the different ice sheet reconstructions used and to the implicit parameterization of basal and terminal melting contained in the calving:water balance relationship used. However, this difference is only important for the concentration of ice-rafted debris (IRD), not its distribution, as the latter is determined by the trajectories. The range of trajectories is produced by the initial size distribution of bergs at each release point. This is chosen according to the flux at the release using modern relationships between iceberg dimensions and size distributions. A full discussion of these relationships is given by *Bigg et al.* [1997].

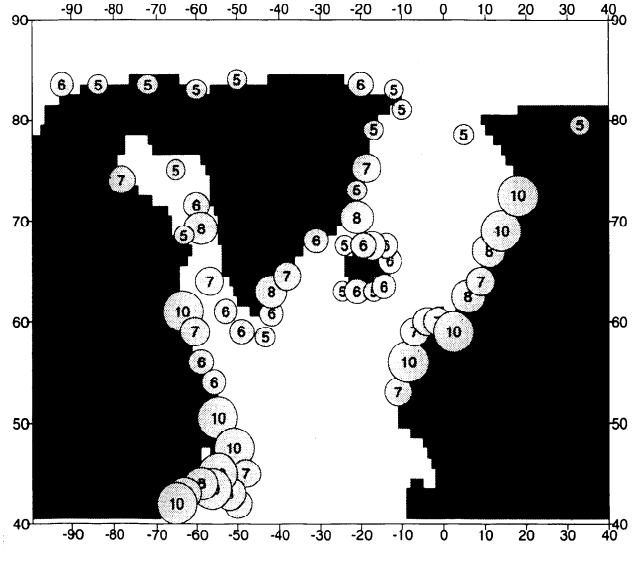

Figure 1. Iceberg release sites for the LGM North Atlantic. Circles mark the centers of regional accumulation from individual glaciers. Actual release points are from the nearest coast (see Figure 4). The radii of the circles are scaled to the distribution of released sizes, with maximum berg size printed inside circle. The sizes are 1, 100 x 67 x 70 m; 2, 200 x 133 x 159 m; 3, 300 x 200 x 240 m; 4, 400 x267 x 320 m; 5, 500 x 333 x 360 m; 6, 600 x 400 x 360 m; 7, 750 x 500 x 360 m; 8, 900 x 600 x 360 m; 9, 1200 x 800 x 360 m; and 10, 1500 x 1000 x 360 m.

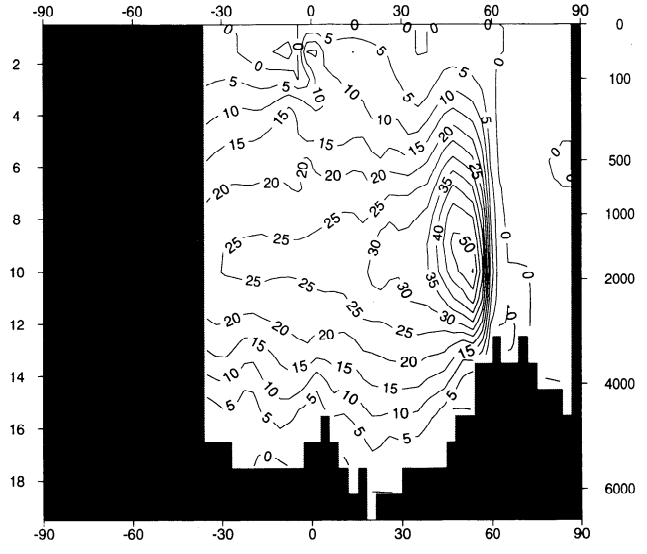

Figure 2. (a) Meridional overturning stream function for the Atlantic Ocean for the coarse resolution northern sinking state (NSS). The contour interval is 5 Sv. (b) Surface potential density for the coarse resolution NSS. The contour interval is 1 kg m^{-3}. Sea ice is shown as a dark mask.

3. Two LGM Model States

3.1. Northern Sinking State

This was the state into which the model naturally fell from the initial fields (see section 2.1). It is characterized by global deep water formation in the North Atlantic with only weak intermediate water formation in both the Indian Ocean sector of the Antarctic and the northwest Pacific. The maximum zonally averaged integrated meridional overturning stream function in the North Atlantic is 55.7 Sv (Figure 2a), roughly 3 times the present-day strength [*Schmitz and McCartney*, 1993] and two thirds stronger than the PDG state of Wadley et al. (unpublished manuscript, 1997). By contrast, there is less than 1 Sv of overturning in either region of intermediate water formation, with the Pacific intermediate water sinking to depths of only a few hundred meters and the Antarctic intermediate water sinking to around 1000 m. While convection occurs across most of the Atlantic from the Labrador Sea just west of the southern tip of Greenland to the European coast at 60°N, the coldest (2.7°C) and saltiest (36.2 psu) water forms in the west of this region with slightly warmer water forming in the northeast Atlantic that subsequently becomes the intermediate water of the basin at depths between 1000 and 2000 m. The densest water forms in the northwest Atlantic because of the combination of extremely cold atmospheric model air temperatures (as low as -20°C, even in the annual average) coming off the ice sheets surrounding the Labrador Sea with relatively high surface salinity (in excess of 36). The large air-sea temperature difference drives very large latent and sensible heat fluxes out of the ocean: over 500 W m^{-2}. By contrast, further east, the air has warmed somewhat because of its oceanic passage, and the heat

loss is significantly less. The north-south atmospheric temperature difference is thus significantly accentuated in the western Atlantic. This combination of low sea surface temperature and high salinity leads to convection. This is stronger than in the PDG state because of the higher salinity at the site of convection (approximately 1.5 psu greater) and the closer proximity to the equator without a ridge system to block the deep return flow.

The state that leads to the maintenance of deep water formation in the Atlantic is contained in Figure 2b, which shows the coarse resolution sea surface density fields. While surface water below 3°C occurs extensively in the Southern Ocean and in the northwest Pacific, as well as the North Atlantic, the saltiest surface waters in the NSS are in the Atlantic and hence so is the densest water. The Pacific, on average, has surface salinities 5-6 psu below those in the Atlantic, giving rise to relatively light water. The source of heat for the thermohaline overturning shown in Figure 2a can be inferred from Figure 3, the global surface velocity field of the coarse resolution model. The Gulf Stream is strong, with much of its flow entering the subpolar gyre of the Labrador Sea, where the densest water is being formed. A subsidiary branch meanders eastward at about 55°N, which we shall call the North Atlantic Drift, supplying the intermediate water formation and, eventually, a northward flowing Norwegian Coastal Current. The water supplying the Gulf Stream ultimately has two sources, both of which are visible in Figure 3: the warm water source from the Pacific Ocean via the Indonesian Throughflow and the Agulhas Current (44%) and the cold water route of detrainment of water from the Antarctic Circumpolar Current (ACC) at the Falklands Confluence (56%).

Another strong feature of the NSS is the pronounced upwelling along the equator in the Atlantic and eastern Pacific caused by the increased trade wind circulation prescribed over these oceans [*Hall et al.*, 1996]. This is visible in the surface divergence in Figure 3 and the density maximum in the equatorial surface waters in Figure 2b. The northern Indian Ocean does not show this feature as the annual mean wind forcing gives a weak boreal summer mean and thus a weak monsoon-like circulation in the ocean.

The North Atlantic Deep Water (NADW) that the NSS forms has a similar temperature to that observed today and a salinity enhanced by 1.1 psu [*Pickard and Emery*, 1986], but a more valid comparison taking account of model inadequacies is with the NADW formed within the PDG state. This is about 3°C warmer and 0.9 psu saltier than that in the NSS. Thus the salinity has changed merely by the lower sea level's concentrating effect while the colder atmosphere has not only moved the zone of deep water formation 1500-2000 km further south but has also led to cooler deep waters. The deep water of the Arctic, however, shows a different signature. Because the present-day (and PDG) NADW has its origins north of the Iceland-Scotland Ridge what enters the main body of the Atlantic is not the densest (and so coldest) water formed but only that that can leave above the sills through this ridge. The deep water of the Arctic is therefore, in both present-day reality [*Schlosser et al.*, 1995] and the PDG state, at a temperature of about -1°C. In the NSS, however, intermediate NADW forms directly south of the Ridge, blocking the penetration of the densest NADW of Labrador Sea origin into the Arctic over the sills into the Norwegian or Greenland Seas. Thus only water at a temperature of 3.5°C can enter the deep Arctic, and so, the NSS predicts a warming there of over 4°C.

The strong Gulf Stream is also reflected in the simulated iceberg trajectories. Figure 4 shows the distribution of meltwater from the full set of iceberg releases over the North Atlantic, weighted to take account of the likely proportion of bergs in each size class, along with trajectories of the 500 x 333 x 360 m bergs. While the debris carried by icebergs is likely to be preferentially near the base, meltwater release can be regarded as a crude proxy for its deposition. Icebergs in the NSS follow distinct tracks. Those from the Labrador Sea either (1) follow the Labrador Current then ground off Newfoundland or, if large and so with plenty of windage, enter the North Atlantic Drift or (2) get entrained in the subpolar gyre in the Labrador Sea with occasional exit eastward where part of the East Greenland Current joins the North Atlantic Drift. Those from the St. Lawrence area get carried north in the Gulf Stream if small or east in the North Atlantic Drift and the atmospheric westerlies if large. Bergs from the Hiberno-

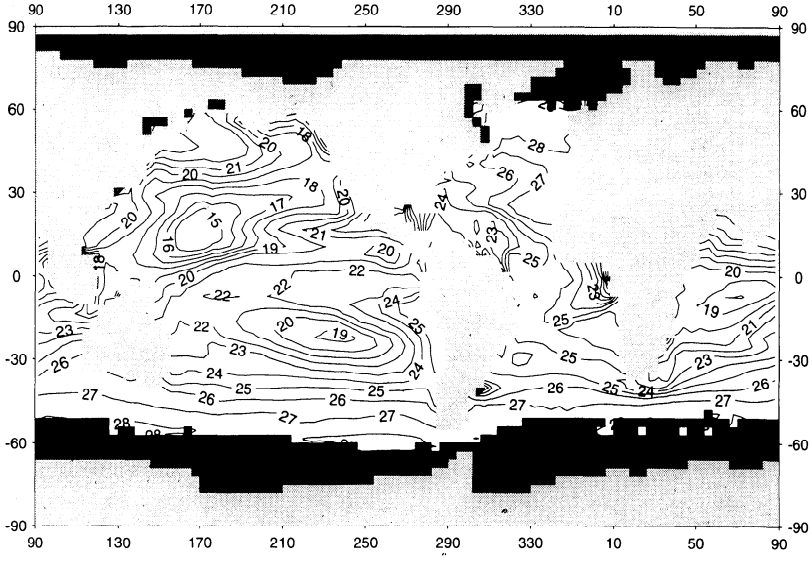

Figure 2. (continued)

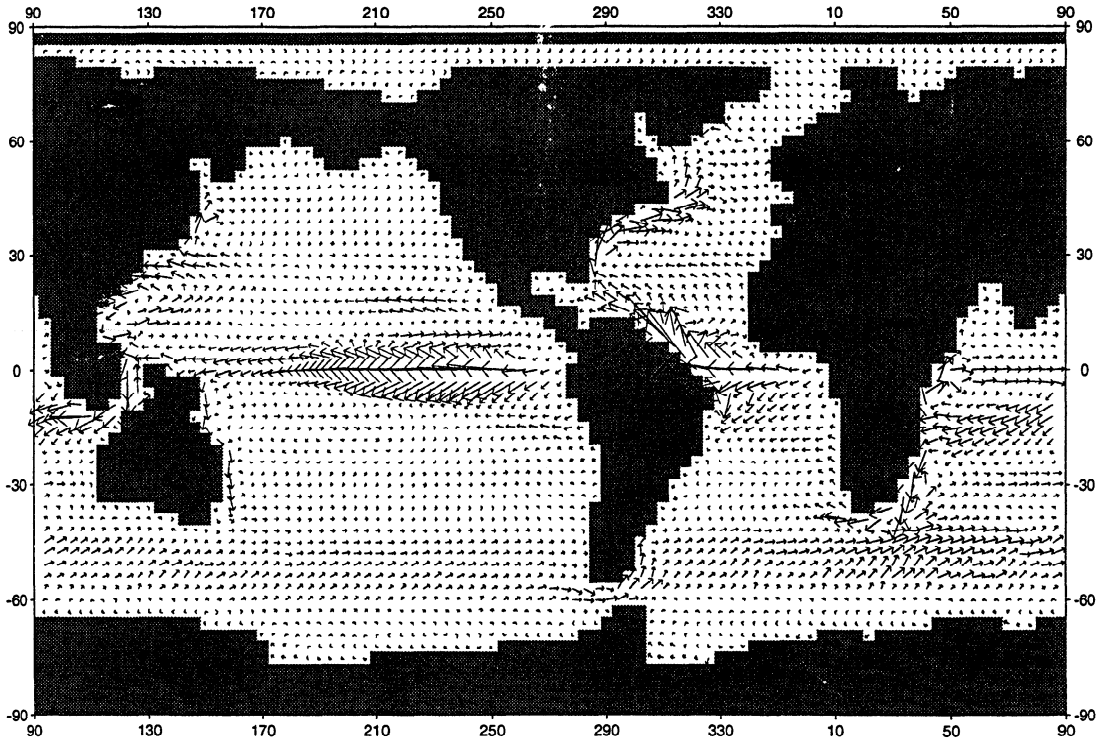

Figure 3. Surface velocity field for the coarse resolution NSS. Arrows of one grid length are 10 cm s^{-1}.

British and Fennoscandinavian ice sheets very rarely move south of the Iceland-Scotland Ridge because of the strong oceanic and atmospheric forcing pushing them northward along the European shore. Icebergs from northeast Greenland also rarely penetrate south of Iceland, but those from southeast Greenland and Iceland can penetrate southward into the central Atlantic in the right combinations of currents and winds.

3.2. Southern Sinking State

This state was entered after adding a freshwater anomaly over the North Atlantic for 500 years and was stable upon its removal (see section 2.1). It is characterized by deep water formation in the Indian Ocean sector of the Antarctic (as can be inferred from Figure 5a), with very little intermediate water formation in the Pacific (0.9 Sv) or North Atlantic (1.6 Sv) (Figure 5a). However, the strength of the global thermohaline circulation is relatively low: only 12.1 Sv of Antarctic Bottom Water (AABW) forms as opposd to the 55.7 Sv for NADW in the NSS. Weak North Pacific intermediate water formation occurs again in the northwest Pacific, while the little NADW formed is generated off northwest Africa as salty (37.6 psu) warm (13°C) water which sinks to 1000-1500 m. No deep water forms at the northern Atlantic ice edge as the water is too fresh here to be denser than the NADW (see the density in Figure 5b). This is reflected in the rather weak Gulf Stream (Figure 6) which separates from the North American coast around 40°N and turns south along the European coast to feed into the NADW formation site off Africa. The near-surface flow in the Atlantic north of the Gulf Stream is slow but predominantly southward.

This Mediterranean-like NADW has two major consequences for the Atlantic. First, it acts as an upper barrier to the colder but fresher water from the Southern Ocean so that this water is kept below 2000 m depth as it spreads into the Atlantic. The deep Arctic therefore can only be filled by NADW as this is the dominant Atlantic water mass at the depth of the sills over the Greenland-Iceland-Scotland Ridge. SSS Arctic water below 500 m is therefore 13°C warmer, although much saltier, than in the PDG state despite the surface is being capped with sea ice. Second, the NADW flows south to form a strong front against, and to mix with, the Antarctic Circumpolar Current around 40°S. This is far enough south for dilute NADW to enter the Indian Ocean beneath the Agulhas Current at depths of 1-2000 m.

A major supplier of heat to deep water formation in the Southern Ocean is the Agulhas Current. In the SSS this completely retroflects south of Africa (Figure 6) to join the Antarctic Circumpolar Current. The deep return cell of the thermohaline circulation is a general spreading, and upwelling, of southern source water throughout the deep Pacific, Indian and Atlantic Oceans. This global deep water is at a temperature of 0.5°-1.0°C and a salinity of 35.65 psu, filling all the basins below 2000 m. The water has very similar properties to modern day Antarctic Circumpolar Deep Water, allowing for the sea level offset in salinity [*Pickard and Emery*, 1986], but is approximately 5°C colder and 0.2 psu fresher than its PDG counterpart. Deep convection is occurring at a more realistic southerly latitude in the SSS case.

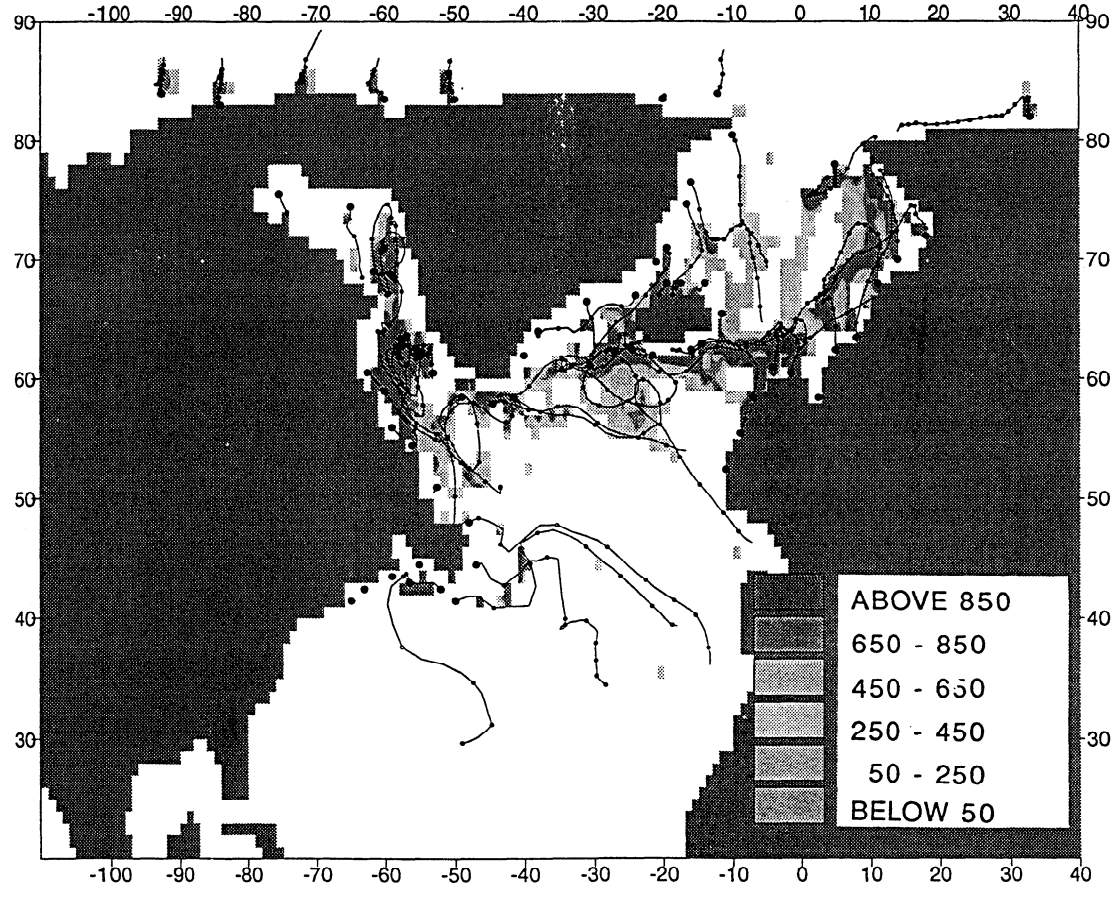

Figure 4. Meltwater distribution from the NSS. The irregular pattern to the south is due to the small number of large bergs reaching these areas. The trajectories of the 500 x 333 x 360 m bergs are also shown. They originate from the large dots, and a small dot occurs on each trajectory at 20 day intervals. The meltwater is a weighted mass, in kilograms, of meltwater added to each square meter of a 1° grid box every 5 days. If the source dot shows no trajectory, it is because coastal grounding occurs within the first 5 days.

The SSS also has a radically different North Atlantic iceberg distribution to the NSS (Figure 7). Partly because of the colder surface waters in this simulation, a small but significant proportion of bergs are able to penetrate much further south in the eastern return arm of the subtropical gyre along the European coast. These bergs come from a number of sources: the Labrador Sea, the St. Lawrence, Hiberno-Britain, Fennoscandinavia, southeast Greenland, and Iceland. The larger the berg, the more remote the source; some of those penetrating furthest south are 1500 x 1000 x 360 m bergs originating from the Barents ice shelf. Because of the weaker Gulf Stream and its steering along 40-45°N, St. Lawrence bergs do not enter the northern North Atlantic. Along the northeast European shore, icebergs move north along the coast, but if sufficiently large, they move offshore and are entrained in the general southward oceanic flow in the Norwegian Sea and northeast Atlantic. Thus the general melting zones for bergs of European origin are very different from those in the NSS.

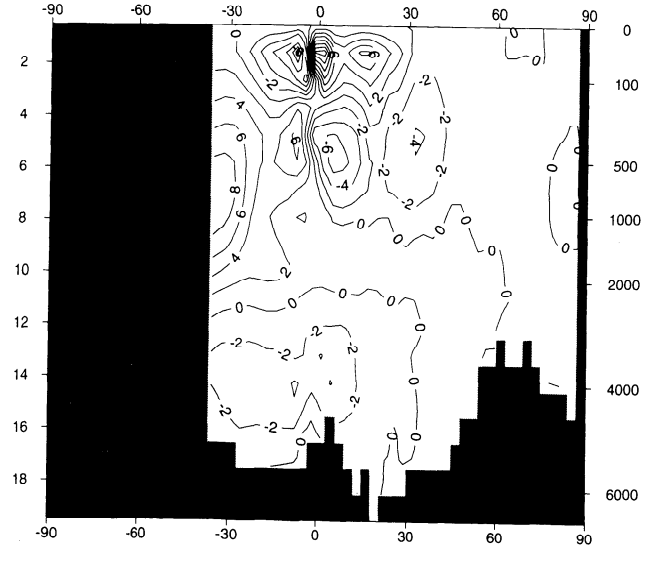

3.3. Comparison of States and Climate: Long-Range Investigation, Mapping, and Prediction

Obvious differences between the NSS and SSS will have been noted by the reader already. The deep water of all basins, except the Arctic, is 1°-2°C colder and 0.5 psu fresher in the SSS than in

Figure 5. (a) Meridional overturning stream function for the Atlantic Ocean for the coarse resolution southern sinking state (SSS). The contour interval is 2 Sv. (b) Surface potential density for the coarse resolution SSS. The contour interval is 1 kg m^{-3}. Sea ice is shown as a dark mask.

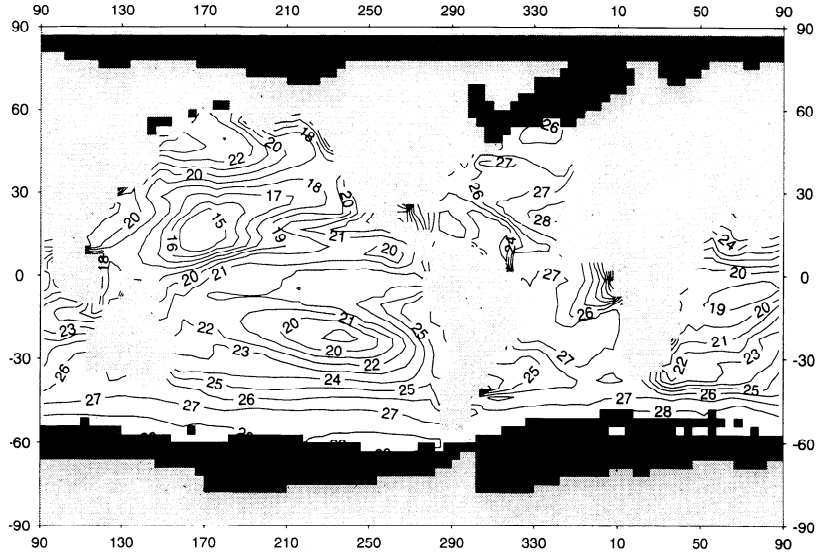

Figure 5. (continued)

the NSS. The Arctic, in contrast, is 14°C warmer and 1.1 psu saltier in the SSS. Intermediate water in the SSS also tends to be colder and slightly fresher, except in the Atlantic where the SSS is dominated by the warm salty NADW.

Near-surface conditions, nonetheless, are very similar in all oceans except the Atlantic (compare Figures 2b and 5b). Outside of the Atlantic, temperatures generally differ by less than 1°C, and salinities differ by less than 0.5 psu, except in the Southern Ocean's formation zone for AABW. Here the front accompanying the merging of the ACC and retroflected Agulhas Current in the SSS tightens and moves equatorward relative to the NSS. Within the Atlantic the intensification of the surface component of the thermohaline circulation in the NSS means that over much of the subtropical and equatorial Atlantic the water, paradoxically, does not warm or salinify as much as in the SSS because it is moving north more quickly. The more northerly penetration of the Gulf Stream and its branches in the NSS, however, leads to much warmer and saltier northern Atlantic surface water. The difference

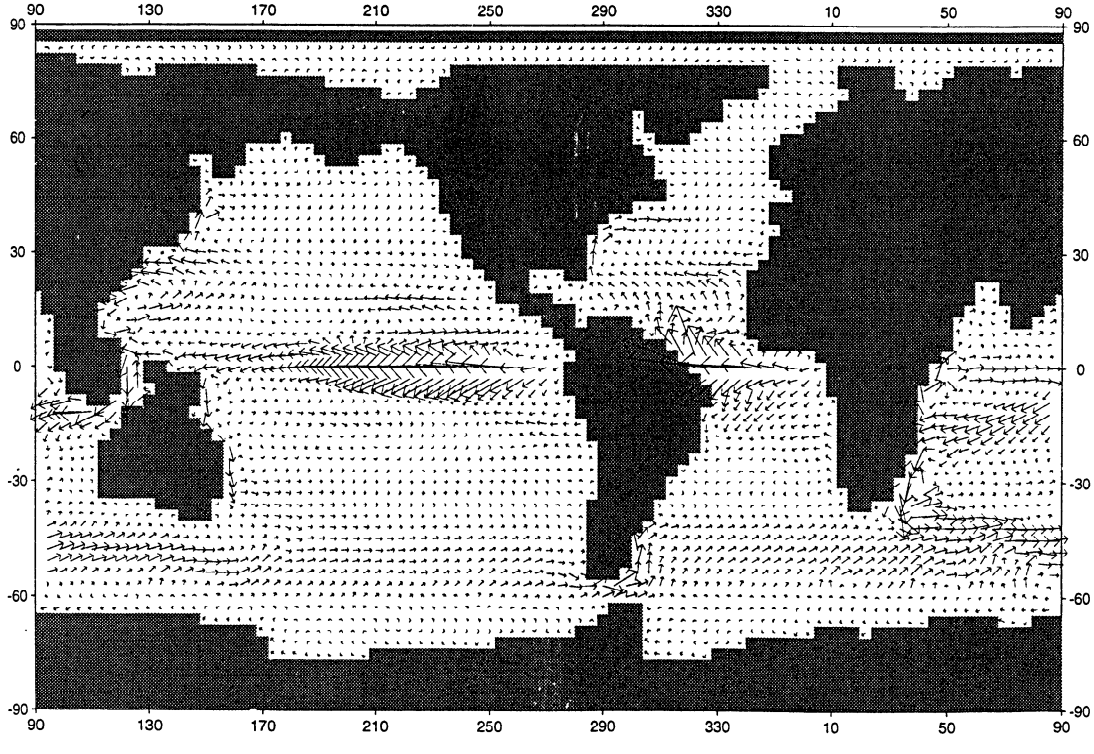

Figure 6. Surface velocity field for the coarse resolution SSS. Arrows of one grid length are 10 cm s^{-1}.

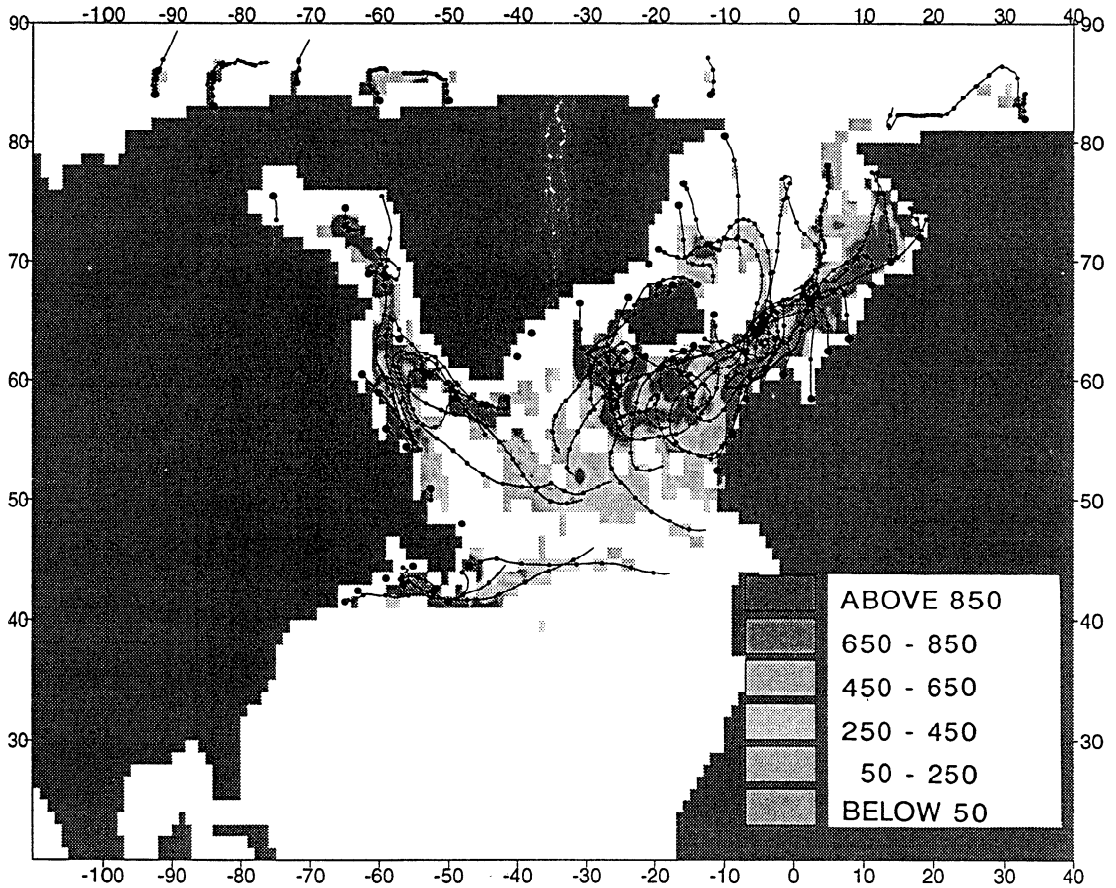

Figure 7. Meltwater distribution from the SSS. The trajectories of the 400 x 267 x 320 m bergs are also shown. See the legend of Figure 4 for more details.

in the global surface velocity field reflects this Atlantic bias by also only differing along the warm water path from the Agulhas Current through the Atlantic into the NSS deep water formation sites around 60°N (compare Figures 3 and 6). The Atlantic iceberg trajectories are a function of this surface current difference. In the SSS, icebergs penetrate further south from more sources in the broad southward current along the European coast, while North American bergs in the NSS tend to get entrained into one of the two branches of the Gulf Stream. European icebergs in the NSS rarely escape from the Norwegian and Greenland Seas.

A comparison of both states with paleoclimatic data is covered in section 4, but it is worth noting the differences and similarities of the two states with the gridded *Climate: Long-Range Investigation, Mapping, and Prediction (CLIMAP)* [1981] sea surface temperature fields here. This is shown in Figure 8 for the NSS. Even though the CLIMAP data were used as the surface forcing for the paleoclimate model of *Hall et al.* [1996], thus indirectly influencing the ocean model's surface temperatures through the bulk aerodynamic fluxes, large regions of the global ocean where the NSS and SSS are similar show distinct differences from CLIMAP. These differences arise because the ocean and atmospheric dynamics in such regions interact in a different manner from that implied by the CLIMAP fields, which, it should be noted, are not necessarily dynamically self-consistent.

The common differences between the NSS and SSS and CLIMAP can be considered in four regional blocks. All equatorial temperatures are 1°-3°C colder than CLIMAP, this difference being most pronounced in the eastern Pacific and west-central Atlantic. The convergence of strong trade winds in the model of *Hall et al.* [1996] leads to marked equatorial upwelling, no doubt strengthened by the known tendency for this type of ocean model to artificially enhance equatorial upwelling. However, this divergence from CLIMAP is consistent with alkenone surface temperature reconstructions in the eastern Atlantic [*Schneider et al.*, 1995] and paleoclimate model results of *Webb et al.* [1997]. Both states, in contrast, show 2°-4°C warmer temperatures along the western coast of the Americas, implying less upwelling than is implicitly supported by CLIMAP. *Mortyn et al.* [1996] also suggest that CLIMAP is in error along the Californian coast, but by being several degrees Celsius too warm, rather than too cold. This suggests that a positive feedback operates between the temperatures in the coastal upwelling zones and the wind strength in a paleoclimate model forced by these conditions: weak upwelling, as implied by *CLIMAP* [1981], leads to even weaker paleoclimate model winds locally and thus warm conditions in the ocean model. An additional divergence from CLIMAP in the Pacific is in the location of the Kuroshio Current. Both the NSS and SSS advect warm water further north off Japan than CLIMAP suggests, with resultant relative warmth over most of the northern Pacific. In both states the Kuroshio separates further north than in the PDG state. This suggests that the difference from CLIMAP is a real model feature, not just a consequence of poor resolution of

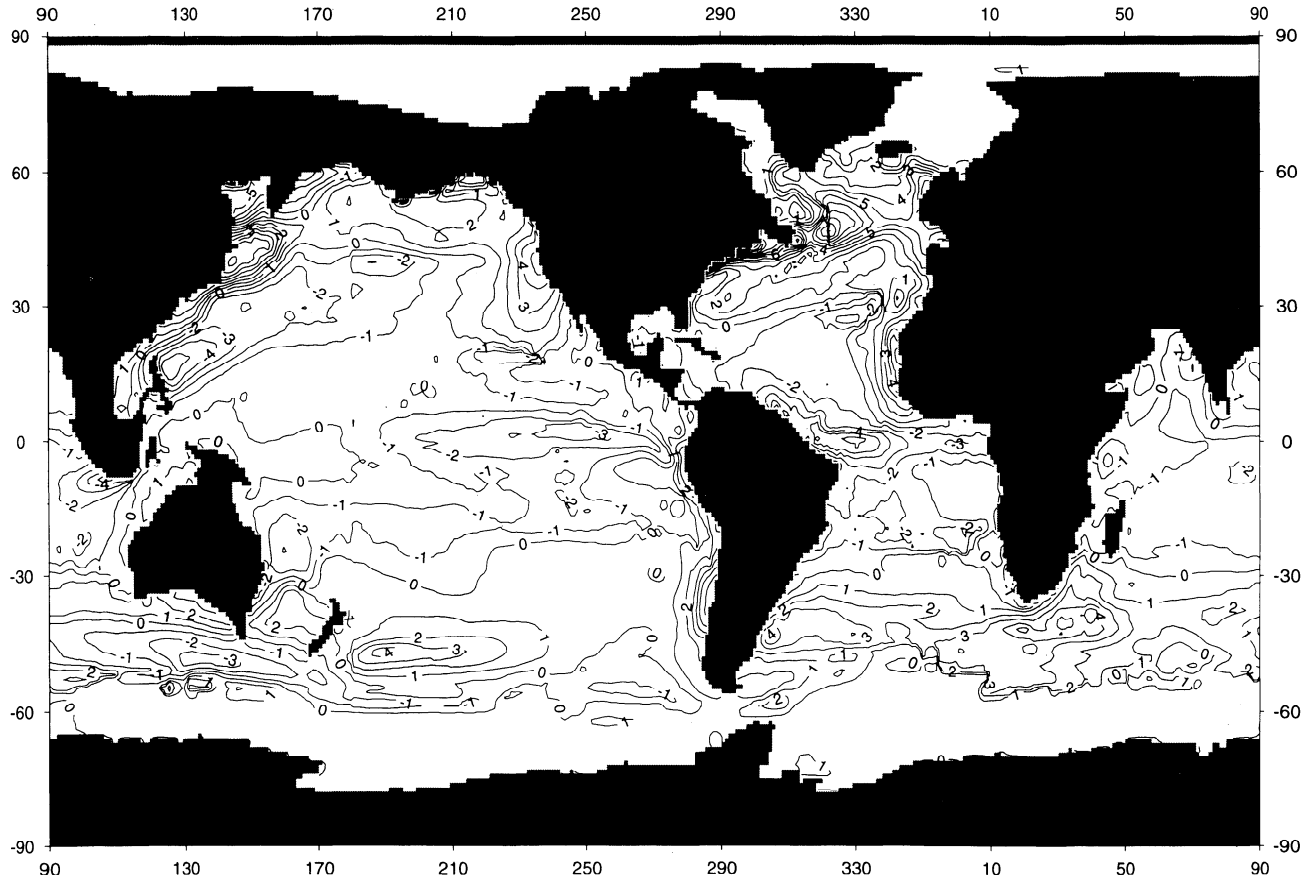

Figure 8. NSS-Climate: Long-Range Investigation, Mapping, and Prediction (CLIMAP) annual mean surface temperature. In the text we highlight the differences that are common to both the NSS and SSS states. The contour interval is 1°C.

the separation region, because a dynamic cause has pushed warm water further north than might be expected. The final regional anomaly between CLIMAP and the two model states is in the Austro-Pacific sector of the ACC. Both model states suggest colder water south of Australia but warmer water in the Tasman Sea and east of New Zealand. This is a region where actual *CLIMAP* [1981] data points were scarce, while the ocean model's ACC is responding dynamically to the bathymetry. Thus the large-scale meandering of the ACC will not be well captured by the mostly zonal contouring of the CLIMAP data in the Southern Ocean.

4. Comparisons With Paleoclimate Data

The purpose of this paper is not to advocate any particular interpretation of the behavior of the global thermohaline circulation at the LGM but to present the dynamical and thermodynamical consequences of two rather different, but possible, modes. However, it is relevant to make some comments on the resemblance of either mode, or components of them, to current reconstructions of LGM oceanic climate, always bearing in mind that the reality of any ocean state is predicated on the accuracy of the prescribed atmosphere in uncoupled simulations.

We have already seen one zone where both models seem consistent with paleo-data, the cooling of equatorial waters, and another where they do not, the lack of cooling in coastal upwelling regions. Both of these are probably directly due to the accuracy of the paleoclimate wind field. A thermodynamical constraint is seen in how well the models reproduce the warm water pool in the western Pacific. Both *Ohkouchi et al.* [1994] and *Thunell et al.* [1994] believed that the LGM warm pool was relatively unchanged in temperature (around 29°C), with *Thunell et al.* [1994] also suggesting that at 30°N or 30°S the temperature was at least 3°C cooler. A comparison with the PDG state of Wadley et al. (unpublished manuscript, 1997), which has a warm pool only 1°C cooler than the observations, shows that differences from the PDG state in both models are consistent with *Thunell et al.* [1994]. The maximum warm pool temperature at the LGM is 28°C (as in the PDG run), with the area bounded by the 27°C isotherm actually larger but the meridional temperature gradient sharpened so that both states are about 3°C cooler by 30°N and 30°S along the western margin. Another region whose surface temperature is largely controlled by thermodynamics rather than by advection is the Caribbean. *Guilderson et al.* [1994] suggest that the LGM Barbados temperature was 4°-5°C cooler; both models show about 2°C cooling relative to the PDG state. In contrast, a region strongly controlled by advection, and very different between the two states, is the North Atlantic. Here the models give mixed signals. Near (20°W, 50°N) *Maslin et al.* [1995] gave estimates of annual surface temperature of about 2°C. This is more consistent

with both the absolute SSS estimate and its difference from the PDG state. The SSS value was also cooler than *CLIMAP's* [1981] data in that region, again consistent with *Maslin et al.'s* [1995] work. In contrast, *Maslin et al's* [1995] reconstruction of surface salinity of about 35.5 psu is very similar to that in the NSS state, and the latter's difference from the PDG state, the SSS salinity being several psu fresher. A different region dominated by advection is the junction of the Atlantic with the Indian Ocean. We have seen that the Agulhas Current is a sensitive indicator of model state. *Pether* [1994] has shown that the Agulhas brought more water into the eastern Atlantic during the LGM. This is strongly suggestive of the intensified North Atlantic-dominated thermohaline circulation of the NSS rather than the quiesent Atlantic of the SSS state.

The emphasis of much relevant paleoceanographic work has been to solve the problem of the state of the LGM thermohaline circulation. Highly relevant to this issue is the sea ice status of the northern Atlantic's marginal seas at the LGM. *CLIMAP* [1981] suggested that even in summer, sea ice extended south of the Greenland-Iceland-Scotland Ridge. More recently, a multitude of evidence suggests that both the Labrador Sea [*Duplessey et al.*, 1988; *Hillairemarcel et al.*, 1994] and the Norwegian Sea [*Hebbeln et al.*, 1994; *Rasmussen et al.*, 1996; *RossellMele and Koc*, 1997] were ice free, at least in the summer. Such conditions are much more consistent with the NSS, where sea ice lies just north of the ridge, as can be implied in Figure 8 (recall that our simulations are of annual means). The NSS is also consistent with Sarnthein et al.'s [1995] reconstruction of a cyclonic gyre in the Norwegian Sea at the LGM. At the other end of the thermohaline circulation the LGM temperature and nutrient content of deep water in the Indian and Pacific Oceans should indicate the origin of such water. *Chappell and Shackleton* [1986] place the LGM deep water temperature in the Pacific 1.5°C colder than today, and *Boyle* [1995] demonstrates that nutrient content in deep LGM Pacific water is greater than in deep Atlantic water by an offset similar to today's. The NSS has deep Pacific water about 2°C colder than the PDG state, while the SSS's Pacific deep water is 4°C colder. Both states' Pacific deep water will have traveled further than any deep water in the Atlantic, whatever its source, so would be enriched in nutrients, although more so in the NSS.

Competition between deep water formation in the Atlantic and Southern Ocean forms the basis of the uncertainty over the state of the LGM thermohaline circulation, as outlined in section 1, although consensus is forming over a view that North Atlantic Deep Water formation was as strong as today, or even somewhat stronger [*Boyle*, 1995; *Yu et al.*, 1996; *Seidov et al.*, 1996], but with NADW being shallower than today and deep water in the Atlantic being made up of water with southern origins [*Labeyrie et al.*, 1992; *Sarnthein et al.*, 1994; *Boyle*, 1995]. Both the NSS and SSS form NADW but with radically different strengths and properties. The latter only forms NADW which is warmer and at shallow depths than *Sarnthein et al.* [1994] would suggest was likely. The rapidly overturning NADW of the NSS, in contrast, forms two types of water: a cool intermediate water in the northeast Atlantic and a cold deep water in the northwest Atlantic. Water deriving from the Antarctic is relatively shallow (see section 3.1). Thus neither state seems to fit the picture painted above. However, the difference in density between the two NADW types in the NSS is sufficient for the densest water to be able only to enter the eastern Atlantic basin through fracture zones in the Mid-Atlantic Ridge in the South Atlantic. Some of this flow enters the eastern basin through the Vema Fracture Zone (10°N), much through the Romanche and Chain Fracture Zones (near the equator) and more through the minima in the African-Antarctic Ridge in the Southern Ocean (0-30°E, 50°S). Thus a north-south cross section in density along 20°W gives the impression of a southern source for the deepest water (see section 5) despite the fact that the eastern Atlantic in this state is being filled with water originating in the Labrador Sea. The NSS is therefore the more compatible state of the two with LGM Atlantic deep water reconstructions and suggests a possible new interpretation of the existing paleoclimate data in the Atlantic.

The final point for comparison is the modeled iceberg meltwater spread and the LGM IRD distribution. *Robinson et al.* [1995] have presented a recent LGM IRD distribution for the NE Atlantic. This has elements compatible with both Figures 4 and 7. The twin routes from North America, from the Labrador Sea and south of Newfoundland, are similar to those for the NSS. The large IRD signal west of the British Isles is suggestive of the southward flux in the SSS. Both states suggest significant deposition in the Norwegian Sea which *Robinson et al.* [1995] show as having an IRD minimum. However, *Ruddiman* [1977], *Kolla et al.*, [1979], and *Bischof* [1994] show LGM IRD deposition as having occurred in this region. The provenance of IRD will give the best differentiation between the two states. Unfortunately, much of the current literature concentrates on IRD from Heinrich events, during which the North Atlantic circulation may have been seriously perturbed from any pre-existing state because of the high influx of freshwater. Here we are concerned principally with the mean non-Heinrich state. *Hebbeln and Wefer* [1997] and *Bischof* [1994] both suggest that LGM debris in the Fram Strait and Norwegian Sea area is consistent with a provenance from the arc from Ireland through Norway to Svalbard. This is more consistent with the NSS. The postulations of sources for two North Atlantic sites, (45°W, 44°N) and (21°W, 49°N), temporally near H2 (the penultimate glacial Heinrich event), by *Gwiazda et al.* [1996] are consistent with either state.

5. Discussion

In this paper we have not proposed either of the two numerically modeled states as being the definitive LGM ocean circulation. Each model has the drawback of not being fully coupled to an atmosphere and of having been driven by annually averaged forcing, which smooths the seasonal extremes actually resulting in polar convection and deep water production. While the NSS seems, on balance, to be consistent with more paleoclimate data than the SSS, the real LGM ocean no doubt lies somewhere else in the phase space of possible thermohaline circulation states. However, the two states raise some interesting fundamental issues about the LGM circulation, and even, as we will see, for pre-Quaternary circulation states.

The thermohaline circulation of the NSS offers the intriguing signature of NADW flowing northward in the eastern Atlantic. If this actually occurred at the LGM, such water, having flowed south through a substantial portion of the western basin, and, in part, even to the Southern Ocean, would have accumulated a higher nutrient signal than either it or the allied intermediate NADW formed in the northeast Atlantic had at source. Thus the $\delta^{13}C$ signal in the deep water of the eastern basin would be de-

pleted in comparison with the overlying intermediate water despite originating from the same general area. Nutrient-rich deep water in the LGM eastern Atlantic is therefore not incompatible with a thermohaline circulation with substantial North Atlantic Deep Water formation.

The two states have been shown to have very similar characteristics, particularly in the upper ocean, in all basins apart from the Atlantic. Given the probable warm bias of the model's deep temperatures, partially derived from the lack of resolution of the seasonal cycle in regions of deep convection, it is hazardous to give too much weight to the difference of a couple of degrees in deep water properties in exploring the paleoclimate data for the deep Pacific and Indian Oceans. However, a major difference between the two models away from the North Atlantic is the behavior of the Agulhas Current. In the NSS, much of this enters the Atlantic, with relatively little retroflection. In the SSS the entire Agulhas Current retroflects to provide the warm water eventually contributing to deep water convection. The actual strength of the Indonesian Throughflow, however, is virtually identical in both states. Thus the southern tip of Africa should be a particularly sensitive area for paleoceanographers to explore further the dilemma of the LGM thermohaline circulation.

Both of our states were stable under the same atmosphere because feedbacks from altered ocean surface conditions could not feed back into the atmospheric model, as would happen in reality. However, the process by which we forced the SSS to appear from the NSS mimics a natural, quasi-periodic forcing in the real glacial ocean, namely, the addition of freshwater to the North Atlantic for several centuries as a result of Heinrich events. It is therefore possible that our two model states are representative of the real glacial ocean between (NSS) and immediately after (SSS) such catastrophes. Climate feedbacks in the heat and freshwater fluxes from the very different North Atlantic surface of the SSS would provide the mechanism to push the real coupled climate from the SSS to the NSS state.

The final feature we wish to discuss is the warm salty NADW source in the SSS. Even though the Southern Ocean produced 90% of the deep water found in this state, sufficient NADW production occurred for very distinctive water to spread out over all of the Atlantic and into the Indian Ocean at intermediate depths. There was also sufficient production for deep basins with relatively shallow sills, the Norwegian and Greenland Seas and the Arctic Ocean, to become filled with this warm, salty NADW. While this very characteristic counts against the SSS's being the LGM thermohaline circulation, very warm deep water is thought to have been present during the Cretaceous [*Crowley and North*, 1991], at least in some areas. Given suitable bathymetry, this model shows that subtropical convection can lead to the presence of extremely different deep water properties in neighboring basins. The distribution of deep water paleotemperatures may therefore have the potential to aid in the reconstruction of paleogeography.

Acknowledgments. We wish to thank P. Valdes for allowing us to use his paleoclimate model results. This work was supported by the NERC NEAPACC Special Topic Grant GST/02/1179.

References

Bigg, G. R., An ocean general circulation model view of the glacial Mediterranean thermohaline circulation, *Paleoceanography, 9*, 705-722, 1994.

Bigg, G. R., M. R. Wadley, D. P. Stevens, and J. A. Johnson, Prediction of iceberg trajectories in the North Atlantic and Arctic Oceans, *Geophys. Res. Lett., 23*, 3587-3590, 1996.

Bigg, G. R., M. R. Wadley, D. P. Stevens, and J. A. Johnson, Modelling the dynamics and thermodynamics of icebergs, *Cold Reg. Sci. Technol., 26*, 113-135, 1997.

Bischof, J., The decay of the Barents ice-sheet as documented in Nordic Seas, *Mar. Geol., 117*, 35-55, 1994.

Boyle, E. A., Cd and C13 paleochemical ocean distributions during the stage 2 glacial maximum, *Annu. Rev. Earth Planet. Sci., 20*, 245-287, 1992.

Boyle, E. A., Last-glacial-maximum North Atlantic Deep Water: On, off or somewhere in between?, *Philos. Trans. R. Soc. London, Ser. B, 348*, 243-253, 1995.

Boyle, E. A., and L. D. Keigwin, North Atlantic thermohaline circulation during the last 20,000 years linked to high latitude surface temperature, *Nature, 330*, 35-40, 1987.

Broecker, W. S., G. Bond, M. Klas, G. Bonani, and W. Wolfli, A salt oscillator in the glacial Atlantic? The concept, *Paleoceanography, 5*, 469-478, 1990.

Bryan, K., Accelerating the convergence to equilibrium of ocean-climate models, *J. Phys. Oceanogr., 14*, 666-673, 1984.

Bryan, F., High-latitude salinity effects and interhemispheric thermohaline circulations, *Nature, 323*, 301-304, 1986.

Chappell, J., and N. J. Shackleton, Oxygen isotopes and sea level, *Nature, 324*, 137-140, 1986.

Climate: Long-Range Investigation, Mapping, and Prediction (CLIMAP), Seasonal reconstruction of the Earth's surface at the last glacial maximum, *Geol. Soc. Am. Map Chart Ser., MC-36*, 1981.

Crowley, T. J., and G. R. North, *Paleoclimatology*, 339 pp., Oxford Univ. Press, New York, 1991.

Dowdeswell, J. A., M. A. Maslin, J. T. Andrews, and I. N. McCave, Iceberg production, debris rafting, and the extent of Heinrich layers (H-1, H-2) in North Atlantic sediments, *Geology, 23*, 301-304, 1995.

Duplessey, J. C., N. J. Shackleton, R. G. Fairbanks, L. Labeyrie, D. Oppo, and N. Kallel, Deepwater source variations during the last climatic cycle and their impact on the global deepwater circulation, *Paleoceanography, 3*, 343-360, 1988.

Fairbanks, R. G., A 17000 year glacio-eustatic sea-level record: Influence of glacial melting rates on the Younger Dryas event and deep-ocean circulation, *Nature, 342*, 637-642, 1989.

Guilderson, T. P., R. G. Fairbanks, and J. L. Rubenstone, Tropical temperature variations since 20,000 years ago: Modulating interhemispheric climatic change, *Science, 263*, 663-665, 1994.

Gwiazda, R. H., S. R. Hemming, and W. S. Broecker, Tracking the sources of icebergs with lead isotopes: The provenance of ocean-rafted debris in Heinrich layer 2, *Paleoceanography, 11*, 77-93, 1996.

Hall, N. M. J., P. J. Valdes, and B. W. Dong, The maintenance of the last great ice sheets: A UGAMP GCM, *J. Clim., 9*, 1004-1019, 1996.

Hebbeln, D., and G. Wefer, Late Quaternary paleoceanography in the Fram Strait, *Paleoceanography, 12*, 65-78, 1997.

Hebbeln, D., T. Dokken, E. S. Andersen, M. Hald, and A. Elverhoi, Moisture supply for northern ice-sheet growth during the last-gacial-maximum, *Nature, 370*, 357-360, 1994.

Hillairemarcel, C., A. Devernal, M. Lucotte, A. Mucci, G. Bilodeau, A. Rochon, S. Vallieres, and G. P. Wu, Carbon productivity and carbon flux in the Labrador Sea during the last 40,000 years, *Can. J. Earth Sci., 31*, 139-158, 1994.

Huang, R. X., Real freshwater flux as a natural boundary condition for the salinity balance and thermohaline circulation forced by evaporation and precipitation, *J. Phys. Oceanogr., 23*, 2428-2446, 1993.

Imbrie, J., et al., On the structure and origin of major glaciation cycles, 1, Linear responses to Milankovitch forcing, *Paleoceanography, 7*, 701-738, 1992.

Kolla, V., P. E. Biscaye, and A. F. Hanley, Distribution of quartz in late Quaternary Atlantic sediments in relation to climate, *Quat. Res., 11*, 261-277, 1979.

Krauss, E. B., Diapycnal mixing, in *Climate-Ocean Interaction*, edited by M. Schlesinger, pp. 269-293, Kluwer Acad., Norwell, Mass., 1990.

Labeyrie, L. D., J. C. Duplessey, J. Duprat, A. Juillet-Leclerc, J. Moyes, E. Michel, N. Kallel, and N. J. Shackleton, Changes in the vertical structure of the North Atlantic Ocean between glacial and modern times, *Quat. Sci. Rev., 11*, 401-413, 1992.

Levitus, S., and T. P. Boyer, *World Ocean Atlas 1994*, vol. 3, *Salinity*, 99 pp., Natl. Oceanic and Atmos. Admin. Natl. Environ. Satell. Data and Inf. Serv., Silver Spring, Md., 1994.

Levitus, S., R. Burgett, and T. P. Boyer, *World Ocean Atlas 1994*, vol. 4, *Temperature*, 117 pp., Natl. Oceanic and Atmos. Admin. Natl. Environ. Satell. Data and Inf. Serv., Silver Spring, Md., 1994.

Lynch-Stieglitz, J., and R. G. Fairbanks, A conservative tracer for glacial ocean circulation from carbon-isotope and palaeo-nutrient measurements in benthic foraminifera, *Nature, 369*, 308-310, 1994.

Maslin, M. A., N. J. Shackleton, and U. Pflaumann, Surface-water temperature, salinity, and density changes in the northeast Atlantic during the last 45,000 years: Heinrich events, deep-water formation, and climatic rebounds, *Paleoceanography, 10*, 527-544, 1995.

Matsumoto, K., An iceberg drift and decay model to compute the ice-rafted debris and iceberg meltwater flux: Application to the interglacial North Atlantic, *Paleoceanography, 11*, 729-742, 1996.

Matsumoto, K., Modeled glacial North Atlantic ice-rafted debris pattern and its sensitivity to various boundary conditions, *Paleoceanography, 12*, 271-280, 1997.

Mortyn, P. G., R. C. Thunell, D. M. Anderson, L. D. Stott, and N. J. Le, Sea-surface temperature-changes in the southern California borderlands during the last glacial-interglacial cycle, *Paleoceanography, 11*, 415-429, 1996.

Ohkouchi, N, K. Kawamura, T. Nakamura, and A. Taira, Small changes in the sea-surface temperature during the last 20,000 years: Molecular evidence from the western tropical Pacific, *Geophys. Res. Lett., 21*, 2207-2210, 1994.

Pacanowski, R. C., K. Dixon, and A. Rosati, *The GFDL Modular Ocean Model Users Guide, Version 1.0, Tech. Rep. 2*, 376 pp., Ocean Group, Geophys. Fluid Dyn. Lab., Princeton, N.J., 1991.

Pether, J., Molluscan evidence for enhanced deglacial advection of Agulhas water in the Benguela Current, off southwestern Africa, *Palaeogeogr. Palaeoclimatol. Palaeoecol., 111*, 99-117, 1994.

Peltier, W. R., Ice age paleotopography, *Science, 265*, 195-201, 1994.

Pickard, G. L., and W. J. Emery, *Descriptive Physical Oceanography*, 4th ed., 249 pp., Pergamon, Tarrytown, N.Y. 1986.

Power, S. B., and R. Kleeman, Multiple equilibria in a global ocean general circulation model, *J. Phys. Oceanogr., 23*, 1670-1681, 1993.

Rahmstorf, S., and J. Willebrand, The role of temperature feedback in stabilizing the thermohaline circulation, *J. Phys. Oceanogr., 25*, 787-805, 1995.

Rasmussen, T. L., T. C. E. van Weering, and L. Labeyrie, High resolution stratigraphy of the Faroe-Shetland Channel and its relation to North Atlantic paleoceanography: The last 87 kyr, *Mar. Geol., 131*, 75-88, 1996.

Robinson, S. G., M. A. Maslin, and I. N. McCave, Magnetic susceptibility variations in Upper Pleistocene deep-sea sediments of the NE Atlantic: Implications for ice rafting and paleocirculation at the last glacial maximum, *Paleoceanography, 10*, 221-250, 1995.

RosellMele, A., and N. Koc, Paleoclimatic significance of the stratigraphic occurrence of photosynthetic biomarker pigments in the Nordic Seas, *Geology, 25*, 49-52, 1997.

Ruddimann, W. F., Late Quaternary deposition of ice-rafted sand in the sub-polar North Atlantic (lat. 40° to 65°N), *Geol. Soc. Am. Bull., 88*, 1813-1827, 1977.

Sarmiento, J. L., and K. Bryan, An ocean transport model for the North Atlantic, *J. Geophys. Res., 87*, 394-408, 1982.

Sarnthein, M., K. Winn, S. J. A. Jung, J. C. Duplessey, L. Labeyrie, H. Erlenkeuser, and G. Ganssen, Changes in east Atlantic deepwater circulation over the last 30,000 years: Eight time slice reconstructions, *Paleoceanography, 9*, 209-267, 1994.

Sarnthein, M., et al., Variations in Atlantic surface ocean paleoceanography, 50°-80°N: A time-slice record of the last 30,000 years, *Paleoceanography, 10*, 1063-1094, 1995.

Schlosser, P., J. H. Swift, D. Lewis, and S. L. Pfirmans, The role of the large-scale Arctic Ocean circulation in the transport of contaminants, *Deep Sea Res., Part II, 42*, 1369-1390, 1995.

Schmitz, W. J., and M. S. McCartney, On the North Atlantic circulation, *Rev. Geophys., 31*, 29-49, 1993.

Schneider, R. R., P. J. Müller, and G. Ruhland, Late Quaternary surface circulation in the east equatorial South Atlantic: Evidence from alkenone sea surface temperature, *Paleoceanography, 10*, 197-219, 1995.

Seidov, D., M. Sarnthein, K. Stattegger, R. Prien, and M. Weinelt, North Atlantic circulation during the last glacial maximum and subsequent meltwater event: A numerical model, *J. Geophys. Res., 101*, 16,305-16,332, 1996.

Semtner, A. J., A model for the thermodynamic growth of sea ice in numerical investigations, *J. Phys. Oceanogr., 6*, 379-389, 1976.

Shackleton, N. S., J. C. Duplessey, M. Arnold, P. Maurice, M. A. Hall, and J. Cartlidge, Radiocarbon age of the last glacial Pacific deep water, *Nature, 335*, 708-711, 1988.

Smith, S. D., Hindcasting iceberg drift using current profiles and winds, *Cold Reg. Sci. Technol., 22*, 33-45, 1993.

Thunell, R., D. Anderson, D. Gellar, and Q. M. Miao, Sea-surface temperature estimates for the tropical western Pacific during the last glaciation and their implications for the Pacific warm pool, *Quat. Res., 41*, 255-264, 1994.

U. S. Naval Oceanographic Office, *Digital Bathymetric Data Base - 5 Minute Grid*, U.S. Nav. Oceanogr. Off., Bay St. Louis, Miss., 1993.

Wadley, M. R., G. R. Bigg, D. P. Stevens, and J. A. Johnson, Sensitivity of the North Atlantic to surface forcing in an ocean general circulation model, *J. Phys. Oceanogr., 26*, 1129-1141, 1996.

Webb, R. S., D. H. Rind, S. J. Lehman, R. J. Healy, and D. Sigman, Influence of ocean heat transport on the climate of the last glacial maximum, *Nature, 385*, 695-699, 1997.

Weeks, W. F., and M. Mellor, Some elements of iceberg technology, in *Proceedings of the First Conference on Iceberg Utilization for Freshwater Production*, edited by A. A. Husseiny, pp. 45-98, Iowa State Univ., Iowa City, 1978.

Yu, E. F., R. Francois, and M. P. Bacon, Similar rates of modern and last-glacial ocean thermohaline circulation inferred from radiochemical data, *Nature, 379*, 689-694, 1996.

Zahn, R., K. Winn, and M. Sarnthein, Benthic foraminiferal 13C and accumulation rates of organic carbon: *Uvigerina peregrina* group and *Cibicidoides wullerstorfi*, *Paleoceanography, 1*, 27-42, 1987.

G. R. Bigg and M. R. Wadley, School of Environmental Sciences, University of East Anglia, Norwich NR4 7TJ, England, U.K. (e-mail: g.bigg@uea.ac.uk)

D. P. Stevens and J. A. Johnson, School of Mathematics, University of East Anglia, Norwich NR4 7TJ, England, U.K.

(Received August 26, 1997;
revised January 30, 1998;
accepted February 4, 1998.)